nature photonics

FOCUS | PROGRESS ARTICLE

PUBLISHED ONLINE: 30 JULY 2010 | DOI: 10.1038/NPHOTON.2010.167

Recent progress in lasers on silicon

Di Liang* and John E. Bowers

Silicon lasers have long been a goal for semiconductor scientists, and a number of important breakthroughs in the past decade have focused attention on silicon as a photonic platform. Here we review the most recent progress in this field, including low-threshold silicon Raman lasers with racetrack ring resonator cavities, the first germanium-on-silicon lasers operating at room temperature, and hybrid silicon microring and microdisk lasers. The fundamentals of carrier transition physics in crystalline silicon are discussed briefly. The basics of several important approaches for creating lasers on silicon are explained, and the challenges and opportunities associated with these approaches are discussed.

The photonics market today is shared by several materials systems, including compound semiconductors (indium phosphide, InP, and gallium arsenide, GaAs), elementary semiconductors (silicon, Si, and germanium, Ge), silica and rare-earth-doped glasses (glass fibre, for example) and polymers. Each system targets particular applications or components. Today, the use of Si photonics is dwarfed by compound semiconductors and Si microelectronics, mostly due to the problems associated with making Si a host material for efficient light emission, and thus subsequently realizing a laser. Fifty years ago the birth of the laser started a scientific and technological revolution. Two years later, diode lasers were demonstrated in group III–V compound semiconductors, and this was around the same time that Si-based transistor radios achieved mass popularity. Since then many scientists and engineers have researched lasing on Si substrates[1]. Rapid advances in Si photonics over the past two decades have been driven not only by the need for more complex, higher functionality and lower cost photonics integrated circuits, but also by pin count and power limits for communications, as summarized in the International Technology Roadmap for Semiconductors (ITRS)[2]. Electronics giants such as Intel, IBM, Hewlett Packard, STMicroelectronics, IMEC and Alcatel-Thales have teamed up with research institutes around the world with support from government, industry and academia to drive progress in Si photonics. The current momentum and potential for making a useful laser in or on Si are significant.

Fundamentals

At the time of the demonstration of the first laser fifty years ago, the fundamental hurdle to realizing stimulated emission in Si was understood: optical transitions must obey the laws of conservation of energy and momentum, but these conditions are not satisfied simultaneously in crystalline Si. In direct bandgap materials (GaAs and InP, for example) radiative recombination occurs rapidly and efficiently via a simple two-particle process, as shown by the simplified band diagram in Fig. 1 (left). Direct bandgap materials have a structure in which the lowest energy points of both the conduction and valence bands line up vertically in the wave vector axis; that is, they share the same crystal momentum. This is the principal reason why GaAs-, InP- and GaN-based materials have been the dominant material systems for semiconductor diode lasers since their first demonstration in 1962.

Si, like Ge, is an indirect bandgap material, and is not naturally capable of accomplishing efficient radiative recombination. Free electrons tend to reside in the X valley of the conduction band, which is not aligned with free holes in the valence band (Fig. 1, right). Therefore if a recombination is to lead to emission of a photon, a third particle must be involved to carry away the excess momentum,

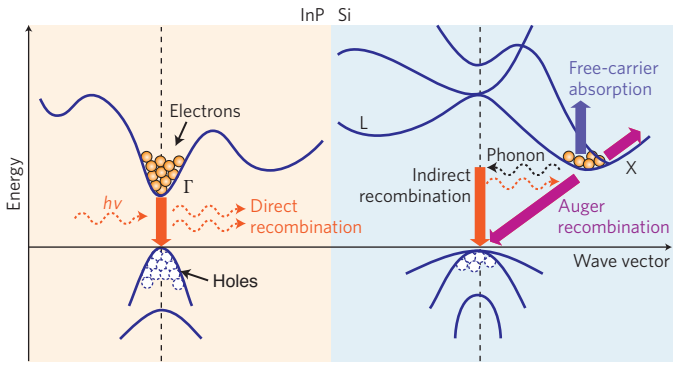

Figure 1 | Energy band diagrams and major carrier transition processes in InP and silicon crystals. In a direct band structure (such as InP, left), electron–hole recombination almost always results in photon emission, whereas in an indirect band structure (such as Si, right), free-carrier absorption, Auger recombination and indirect recombination exist simultaneously, resulting in little photon emission.

which results in slow optical transition rates. A major non-radiative process is Auger recombination, in which an electron (or hole) is excited to a higher energy level by absorbing the released energy from an electron–hole recombination. The Auger recombination rate increases with injected free-carrier density and is inversely proportional to the bandgap. Free-carrier absorption (FCA) represents another major non-radiative process wherein the free electrons in the conduction band can jump to higher energy levels by absorbing photons. In high-level carrier injection devices (lasers and amplifiers, for example) or heavily doped layers, free-carrier loss is orders of magnitudes higher than the material gain[1]. For both Auger recombination and FCA, the electrons pumped to higher energy levels release their energy through phonons, rather than by emitting photons. They also have much shorter lifetimes (τ_{nonrad}) than those of radiative processes (τ_{rad}) in Si, resulting in an extremely poor internal quantum efficiency η_i of light emission, which is defined as[3]

$$\eta_i = \frac{\tau_{nonrad}}{\tau_{nonrad} + \tau_{rad}}$$

and is generally of the order of 10^{-6}. Consequently, semiconductor laser research over the past fifty years has primarily focused on compound semiconductor substrates, but now there is intense interest in lasers on Si.

Department of Electrical and Computer Engineering, University of California, Santa Barbara, California 93106, USA. *e-mail: dliang@ece.ucsb.edu

NATURE PHOTONICS DOI: 10.1038/NPHOTON.2010.167

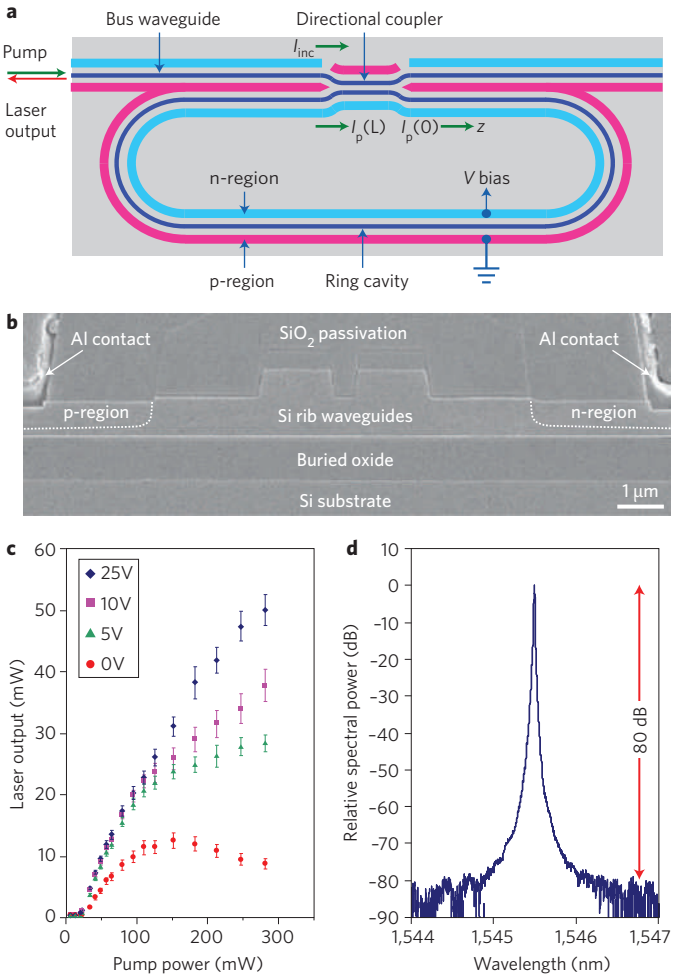

Figure 2 | Low-threshold Si Raman racetrack ring laser. a, Schematic of a device with a p-i-n junction design. $I_p(0)$ and $I_p(L)$ are the pump power at the starting point and after a round trip in the cavity, respectively. The light propagation direction is given by *z*. **b**, SEM cross-section of a directional coupler and p-i-n junction region. **c**, Laser output power against coupled input pump power, showing a higher output power achieved at a higher reverse bias on p-i-n junction for a 3 cm cavity. The error bars here are derived from different measurement traces. **d**, High-resolution spectrum showing a low-threshold Si Raman racetrack ring laser with a side-mode suppression ratio of over 70 dB. Figure reproduced from ref. 25, © 2007 NPG.

The recent and widespread availability of nanotechnology has allowed the traditional phonon-selection rule in indirect bandgap materials to be relaxed by breaking the crystal-symmetry or by phonon localization through the creation of nanostructures in crystalline Si. The motivation is to achieve quantum confinement of excitons in a nanometre-scale crystalline structure[4]. A number of groups have reported enhanced light-emitting efficiency and optical gain in low-dimensional (that is, of the order of the de Broglie wavelength) Si at low temperatures. They include porous Si[5–8], Si nanocrystals[9–12], Si-on-insulator (SOI) superlattices[13] and photonic-crystal-like nanopatterns[14], and Si nanopillars[15,16]. However, achieving room-temperature continuous-wave (CW) lasing based on these temperature-dominated processes remains a challenge[3,17,18].

Despite being fundamentally limited by an indirect bandgap and low mobility, Si exhibits a number of important properties that make it a good substrate, if not necessarily a good gain medium for diode lasers. First, Si wafers are incredibly pure and have low defect density. Second, state-of-the-art 32 nm complementary metal–oxide–semiconductor (CMOS) technology is sufficiently advanced to fabricate virtually all Si photonic components, which are mostly still in the micrometre regime. Both factors allow for Si waveguides with propagation losses that are typically one order of magnitude lower than compound semiconductor waveguides. Furthermore, Si has a high thermal conductivity, which is a very useful characteristic for an active device substrate. SiO_2, the high-quality native oxide of Si, serves as a protective layer and a naturally good optical waveguide cladding, owing to its large refractive index difference from Si ($\Delta n \sim 2.1$). This is one of the major advantages of Si over Ge and other semiconductors for use in integrated circuits. Further loss-reduction in Si waveguides by oxidation[19] and hosting rare-earth doping in SiO_2 brings additional benefits to passive Si lightwave circuits. Although low waveguide loss does not change the ultralow band-to-band radiative emission efficiency in Si, it improves the efficiency of Si lasers that rely on a nonlinear effect such as Raman scattering.

Silicon Raman lasers

The Raman effect refers to the inelastic scattering of a photon by an optical phonon. When incident light is absorbed by an atom or molecule at a vibrational state, the system energy is raised to an intermediate higher state. In most cases, the energy quickly drops back to the original vibrational state by releasing a photon with the same frequency, which is known as Rayleigh scattering, and is analogous to elastic scattering. Yet it is also possible to observe very weak (approximately one in ten million photons) additional components with lower and higher frequencies than the incident light due to the absorption or emission of optical phonons, namely the Stokes and anti-Stokes transitions, respectively.

If a scattering medium is irradiated with pump and signal beams simultaneously, the pump beam excites the constituent molecules or atoms to a higher vibrational level, while the signal beam, which has a frequency resonant at the Stokes transition, triggers the generation of another Raman Stokes photon. Thus, amplification can be achieved through stimulation of the Stokes transition. This technique is known as stimulated Raman scattering, and has enabled the realization of Raman glass fibre amplifiers with gain bandwidths of over 100 nm. The Raman gain coefficient in Si is around five orders of magnitude larger than that in amorphous glass fibres because of the well-organized single-crystal structure[20]. However, Si waveguide loss is also several orders of magnitude higher than in glass fibre, making fabrication of a low-loss Si waveguide one of the keys to realizing net Raman gain in Si. Furthermore, the tight optical confinement in an SOI waveguide leads to an ultrasmall waveguide effective area, which in turn lowers the pump power threshold for stimulated Raman scattering. A pump with energy well below the Si bandgap is typically used to avoid elevating the electrons up to the conduction band and also to suppress FCA — both of which prevent lasing in Si. Initial studies demonstrated up to 0.25 dB of stimulated Raman gain for a Stokes signal at 1,542.3 nm for SOI waveguides, using a 1,427 nm pump laser with a CW power of 1.6 W (ref. 21). Such high pump powers, however, induce another optical loss mechanism — two-photon absorption (TPA). TPA is a nonlinear loss mechanism in which two photons combine their energies to boost an electron in the valence band to the conduction band. Free carriers further induce FCA and dump more optical power inside the cavity. TPA increases with the number of photons in a waveguide, and therefore becomes a limiting factor when using high optical pump powers. The first demonstration of a pulsed Si Raman laser[22] overcame TPA by using a long delay together with a short optical pulse, thus allowing the carriers generated during TPA to recombine prior to the next pass of the optical pulse. Following demonstrations used a p-i-n (p-type/intrinsic/n-type layers) structure in the waveguide to sweep free carriers away under

a reverse bias[23], as this reduced the free-carrier lifetime to minimize TPA-induced FCA. An alternative method involved reducing the volume-to-surface ratio of the waveguide to increase the surface recombination rate of the carriers. The first successful demonstration of a CW Si Raman laser followed soon after[24], with a lasing threshold at an effective pump power of ~182 mW for a reverse bias of 25 V.

The threshold pump power was recently reduced using a high *Q*-factor racetrack ring resonator cavity and an optimized p-i-n diode structure[25]. The cavity resonance effect enhances the light field inside cavity. Figure 2a is a top-view schematic of the racetrack ring cavity, with the p-i-n regions highlighted. A large bend radius of 400 μm helps to minimize waveguide bending losses, even though high-index-contrast SOI waveguides can typically support low-loss light propagation in a more compact bending structure. To utilize the pump power efficiently and achieve a low lasing threshold, the directional coupler in the 1.6-cm-long bus waveguide is designed so that it is close to the critical coupling for the pump wavelength (1,550 nm) but has low coupling for the Stoke signal wavelength (1,686 nm). The narrow gap in the evanescent coupler was filled with boron phosphorus Si glass to eliminate any air voids that form, which helps to reduce losses. A thin layer of SiO_2 buffer layer on top of the Si surface is deposited before coating with boron phosphorus Si glass to prevent phosphor and boron from diffusing into the Si during the thermal reflow step and inducing FCA later on[25].

TPA-induced FCA nonlinear optical loss can also reduced by optimizing the p-i-n reverse-biased diode. Balancing the trade-off between a good metal/Si contact and induced free-carrier absorption loss ensures that the diffusion of electrons and holes under reverse bias produces a uniform field across the optical mode, which allows efficient carrier removal without significantly increasing the linear optical loss. Figure 2b shows a scanning electron microscopy (SEM) cross-sectional image of the directional coupling region and incorporated p-i-n diode structure. The average optical loss of this particular racetrack ring was measured to be 0.20 ± 0.05 dB cm^{-1}, which indicates a negligible contribution of the p-i-n diode to the linear propagation loss when the p- and n-region separation is greater than 6 μm (ref. 25). An extremely short free-carrier lifetime of <0.4 ns was obtained for this device, resulting in a substantial reduction in the lasing threshold. Under a reverse bias of 25 V, the laser had a threshold of 20 mW and a maximum output power of 50 mW (Fig. 2c). These represent five- and tenfold improvements, respectively, over the first CW Si Raman lasers[24]. As the bias voltage is lowered, the laser output begins to saturate earlier, owing to the relatively longer effective carrier lifetime. However, the lasing threshold changes only slightly because the TPA-induced FCA is much weaker at lower pump powers around the threshold. Silicon Raman lasers benefit significantly from high spectral purity, which results from the absence of a linewidth enhancement (a common effect in diode lasers). For example, linewidths of <100 kHz and side-mode suppression ratios of over 70 dB (see Fig. 2d) are well beyond the best performance of present diode lasers[25].

Epitaxial lasers on silicon

Compared with Si, GaAs and InP have lattice mismatches of 4.1% and 8.1%, respectively, and thermal expansion coefficient mismatches of 120.4% and 76.9%, respectively. These result in a threading or misfit dislocation density of 10^8–10^{10} cm^{-2} when either compound is grown on a Si substrate[26]. Numerous approaches, including special surface treatment[27], strained superlattices[28,29], low-temperature buffers[30] and growth on patterned substrates[31] have been used to reduce the dislocation density to around 10^5–10^6 cm^{-2}, but this is still around two orders of magnitude higher than in InP- or GaAs-based epitaxial wafers for room-temperature CW lasers. Recent advanced epitaxial techniques with SiGe[32,33] and GaSb[34] buffer layers have enabled the realization of GaAs-based CW diode lasers on Si substrates at room-temperature. However, their reliability still remains a big issue for any future practical application. An exciting approach is the epitaxial growth of compound semiconductors lattice-matched to Si, such as GaNAsP[35,36].

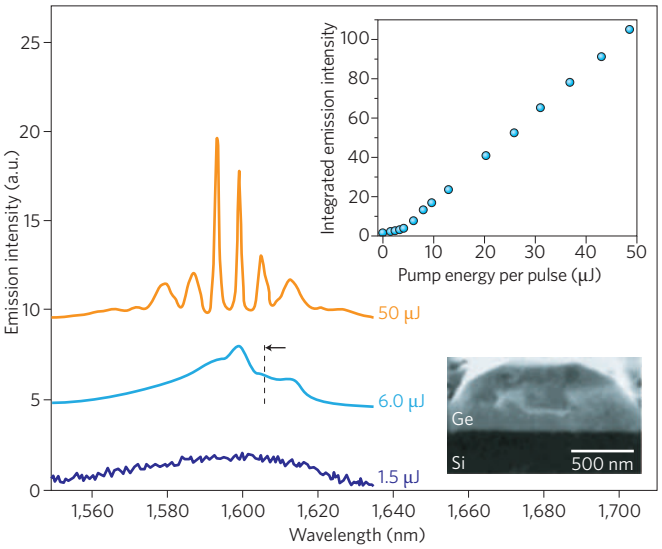

Figure 3 | Optically pumped Ge-on-Si laser demonstrating CW operation at room temperature. Edge-emission spectra of a Fabry–Pérot Ge waveguide under three different levels of optical pumping from a *Q*-switched laser at 1,064 nm with a pulse duration of 1.5 ns and at a repetition rate of 1 kHz is shown. The arrow indicates the peak optical gain wavelength. Top inset: integral emission intensity from the waveguide facet versus optical pump power, showing the lasing threshold. Bottom inset: cross-sectional SEM image of the Ge waveguide. Figure reproduced with permission from ref. 45, © 2010 OSA.

Another exciting approach is Ge-on-Si (or SiGe-on-Si) epitaxial growth. Key photonic components from this material system, including p-i-n[37] and avalanche photodetectors[38,39] and modulators[40,41], have demonstrated performances comparable or even better than their III–V counterparts in certain aspects. Pure Ge has a significant mismatch with Si in terms of its lattice constant and thermal expansion coefficient. Germanium has an indirect band structure, but the energy gap (0.8 eV) from the top of the valence band to the momentum-aligned Γ valley is close to the actual bandgap (0.66 eV), which increases the chance of radiative recombination between the Γ valley and the valence band. The larger thermal expansion coefficient of Ge naturally leaves thermal tensile strain in Ge after growth on a Si substrate, and a moderate tensile strain of 0.2–0.25% is able to reduce the energy difference between the Γ and L valleys to 115 meV (refs 42,43). In addition, strain raises the light-hole band, which increases optical gain for high injection[42]. Free electrons, incorporated through heavy n-doping, quickly fill up the L valley to a level equal to that of the Γ valley, which increases the probability that those free carriers will begin to occupy the Γ valley for radiative recombination. These techniques have enabled room-temperature direct-bandgap electroluminescence[43,44] and CW room-temperature optically pumped operation of Ge-on-Si lasers[45].

The first Ge-on-Si laser operating at room-temperature was fabricated by selectively growing 1.6 μm × 0.5 μm Ge waveguides epitaxially on Si (ref. 45). A thermally induced tensile strain of 0.24%, together with a phosphorous doping level of 1×10^{19} cm^{-3}, allowed enhanced light emission from direct gap of 0.76 eV. A cross-sectional SEM picture of the Ge waveguide is shown in the inset of Fig. 3. The

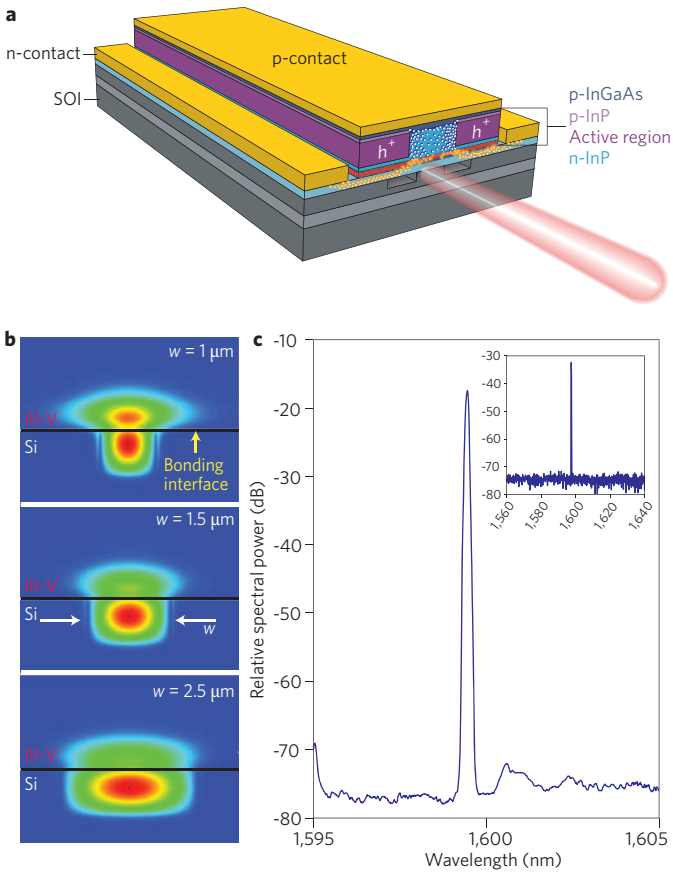

Figure 4 | Hybrid Si device platform and hybrid Si distributed feedback lasers. a, Schematic of a hybrid Si Fabry–Pérot laser, showing recombination scheme of injected carriers in III–V epitaxial layers on top of a Si waveguide. **b**, Simulated hybrid mode profiles at different Si waveguide widths, *w*, showing that modal confinement in Si (III–V) increases (decreases) as the waveguide width increases. **c**, Spectra of a hybrid Si distributed feedback laser, showing a side-mode suppression ratio of 50 dB and a single-mode bandwidth of over 100 nm (inset). Figure **c** reproduced with permission from ref. 55, © 2008 OSA.

study involved optically pumping a mirror-polished, 4.8-mm-long Fabry–Pérot cavity with a 1,064 nm *Q*-switched laser of 1.5 ns pulse duration. The actual peak pump power density absorbed by the Ge was estimated to be 300 kW cm^{-2}. A broad photoluminescence peak at 1,600 nm was observed under pumping at 1.5 μJ per pulse, with emission peaks emerging at 1,599, 1,606 and 1,612 nm. A shoulder is visible at 1,594 nm when the pump increases to 6.0 μJ per pulse, which corresponds to the lasing threshold in the inset of Fig. 3.

In contrast with bulk direct-bandgap compound semiconductors, an interesting and important characteristic in strained Ge is the enhanced luminescence efficiency at high injection levels and high temperatures[44]. The theoretical explanation of the larger overlap of the Fermi–Dirac distribution in the Γ valley due to Joule heating has been confirmed experimentally by electrically driven Ge-on-Si LEDs[44]. Researchers are currently investigating an electrically pumped version of the Ge laser consisting of a Si/Ge/Si heterostructure diode that is p$^+$-, n$^+$- and n-doped, respectively.

Rare-earth-doped Si/SiO_2 light-emitting devices

Silicon-based structures that use rare-earth-ion 'guests' in a dielectric 'host' have great potential for lasing at telecommunications wavelengths. Researchers have recently reported that an electrically pumped rare-earth-ion laser on Si is nearing realization[46,47]. This p-i-n diode structure consists of a stack of very thin Si layers alternating with very thin erbium-doped SiO_2 layers. Carriers injected laterally into the Si films make their way into the oxide films to excite the erbium. Related work on Si LEDs also shows promise[11,12]. By introducing dislocation loops into Si along with erbium implantation, room-temperature electroluminescence and optical gain at a wavelength of 1.5 μm have been achieved. Similarly, in related experiments, strong electroluminescence at 1.2–1.3 μm has resulted from replacing the boron implanted in Si with thullium.

Hybrid silicon lasers

The SOI substrates used in Si photonics are usually made by wafer bonding an oxidized Si wafer onto another Si carrier wafer. By wafer-bonding compound semiconductors to SOI substrates, this same approach can be used to combine the superior gain characteristics of compound semiconductors with the superior passive waveguide characteristics of Si waveguides. This idea has been demonstrated for wafer sizes of up to 150 mm in diameter, and the photoluminescence characteristics of the bonded compound semiconductor films actually improve after bonding, probably due to the release of strain during cooling after epitaxial film growth[48,49]. In this way, it is possible to combine epitaxial films with low threading dislocation densities to the lattice-mismatched Si substrate. This has advantages over bonding individual III–V lasers to a SOI host substrate[50,51]. Shown schematically in Fig. 4a, the Si passive lightwave circuits are patterned prior to the transfer, and the III–V films are processed after transfer using standard lithography-based patterning techniques used to fabricate III–V lasers[52]. Lateral current confinement is achieved using h$^+$ proton implantation. The mode is confined predominantly in the Si waveguide, with a fraction (typically 3–8%) contained in the III–V quantum wells, thus forming a hybrid mode.

The confinement factor can be dramatically changed by changing the waveguide width (Fig. 4b); when the Si waveguide width increases, the mode tends to sink more into the Si, which decreases confinement in the III–V layer. This allows lasers, amplifiers, and photodetectors with different quantum-well confinement factors to be integrated onto the same chip.

Following the demonstration of hybrid Fabry–Pérot lasers at room-temperature[51,52], non-Fabry–Pérot cavity devices[53–57] were soon fabricated for on-chip light sources, including for distributed feedback, distributed Bragg reflector and segmented grating distributed Bragg reflector lasers. A single mode (>100 nm bandwidth) spectrum with a side-mode suppression ratio of 50 dB (Fig. 4c) from a hybrid Si distributed feedback laser is comparable to those based on III–V materials[55].

For optical interconnects, small size, low power consumption and a short cavity design are all critical. Compact microring lasers with diameters of 15–50 μm have been fabricated through a self-aligned process, allowing CW operation up to a stage temperature of 65 °C (ref. 57). Figure 5a shows a schematic of an electrically pumped microring resonator laser, its cross-section SEM image, and a simulated fundamental transverse electric mode, showing the shift to the waveguide edge. CW thresholds as low as 4 mA with reasonable output powers (3.5 mW) have been observed in devices with diameters of 50 μm (ref. 57). Further reducing the laser diameter and increasing the facet reflectivity (that is, reducing the mirror loss for straight devices and the outcoupling for ring/disk devices) results in a drastic reduction in the threshold. The dotted line in Fig. 5b shows how the threshold has decreased from previously demonstrated large hybrid Si racetrack ring lasers (blue dot)[53] to the recently fabricated microring lasers[57] and eventually to ultracompact devices with diameters of 4.5 μm and thresholds of ~400 μA (red dot). Figure 5c shows a photo of two 1 cm^2 chips,

each containing ~400 devices lying aside a portion of a 150-mm-diameter hybrid Si racetrack laser wafer[58]. Thanks to this reduction in size, the fabrication of millions of microring lasers on a single Si wafer is now feasible.

Sub-milliampere-threshold CW lasing has been experimentally demonstrated on a hybrid III–V-on-Si integrated platform[56] similar to the hybrid microring laser discussed above. By lasing inside a compact microdisk III–V cavity and coupling to an external Si waveguide, a good overlap between the optical mode and electrical gain results in threshold currents as low as 350 μA (ref. 59). An SOI waveguide is positioned underneath the III–V microdisk to capture a small fraction of the evanescent light vertically (Fig. 6a). Four devices with slightly different cavity lengths integrated onto the same Si waveguide (Fig. 6b) will have different resonance wavelengths, allowing such a waveguide to be used as a wavelength-division multiplexing source[60]. The spectrum in Fig. 6c results from combining four devices with diameters of 7.632, 7.588, 7.544 and 7.5 μm. The devices are individually tuned to give an even spread inside one free spectral range (~24 nm)[60]. However, increasing thermal impedance causes laser performance to decrease dramatically[60,61] with smaller diameters, which is a major hurdle in the realization of compact devices.

Challenges and opportunities

Lasers on Si are now a reality, and the recent progress in making Si lase — regardless of the particular lasing mechanism — is exciting. Although the gain in nanoscale Si at low temperatures diminishes quickly before reaching room temperature, and despite the generated photon energy being larger than or similar to the Si bandgap, steady progress is being made. Erbium-doped Si nanocrystals push emission to telecommunication wavelengths, and the use of a metal–oxide–semiconductor structure results in an electroluminescence efficiency that is comparable to commercial III–V LEDs. As long as a good trade-off solution between efficiency and lifetime can be found, lasers on Si will find applications in relatively low-speed, large-volume optical interconnects. Materials scientists are pursuing a variety of heteroepitaxy techniques to find a way to reduce the dislocation density in compound semiconductors on Si to a level that is low enough for good and reliable laser performance. The recent demonstration of optically pumped Ge-on-Si lasers is exciting, and is focusing attention on how to increase the gain to levels comparable to that of III–V materials. Hybrid III–V-on-Si technology currently has the most advanced devices and the most advanced photonic integrated circuits on Si. Wafer-scale III–V epitaxial transfer up to 150 mm in diameter[58] and individual III–V dyes attaches to larger SOI wafers[62] show high-volume manufacturability. Monolithic methods are typically preferred, although the highest quality SOI wafers today are made by wafer bonding. The ultimate reliability, performance, uniformity and cost of the hybrid approach are still unknown.

New opportunities continue to appear. Companies are now considering whether optical interconnects could be a possible solution to the problems of high power consumption and low bandwidths of electrical interconnects, while also achieving smaller interconnect delays, lower cross-talk and better resistance to electromagnetic interference. For example, it is challenging to extend the reach of a 10 Gb s^{-1} copper interconnect beyond 30 cm, even with sophisticated electronic processing. Placing a wavelength-division multiplexing optical communication system in or between microprocessors allows theoretically terahertz bandwidths for on- and off-chip interconnections. Low-cost optical interconnects will be manufactured in much higher volumes than they are today when applied to diverse applications such as high-definition display ports, memory server interconnects and on/off-chip interconnects. The emerging market of fibre-to-PC devices using diplexers and triplexers, which require the integration of lasers and photodetectors with passive multiplexers and demultiplexers, could be a more immediate application of existing technology. For example, a hybrid Si integrated triplexer containing a 1,310 nm laser for upstream data transmission as well as 1,310/1,500 nm and 1,490/1,550 nm wavelength selective splitters and photodetectors for downstream digital and video reception was recently demonstrated by transferring two types of III–V epilayers onto a single Si chip[63]. Quantum-well intermixing is a promising option that avoids bonding two different III–V materials simultaneously and so has enabled integration of hybrid lasers and modulators[64]. Over time, hybrid photodetectors will probably be replaced by monolithic Ge detectors. The ultimate integration scheme in practical

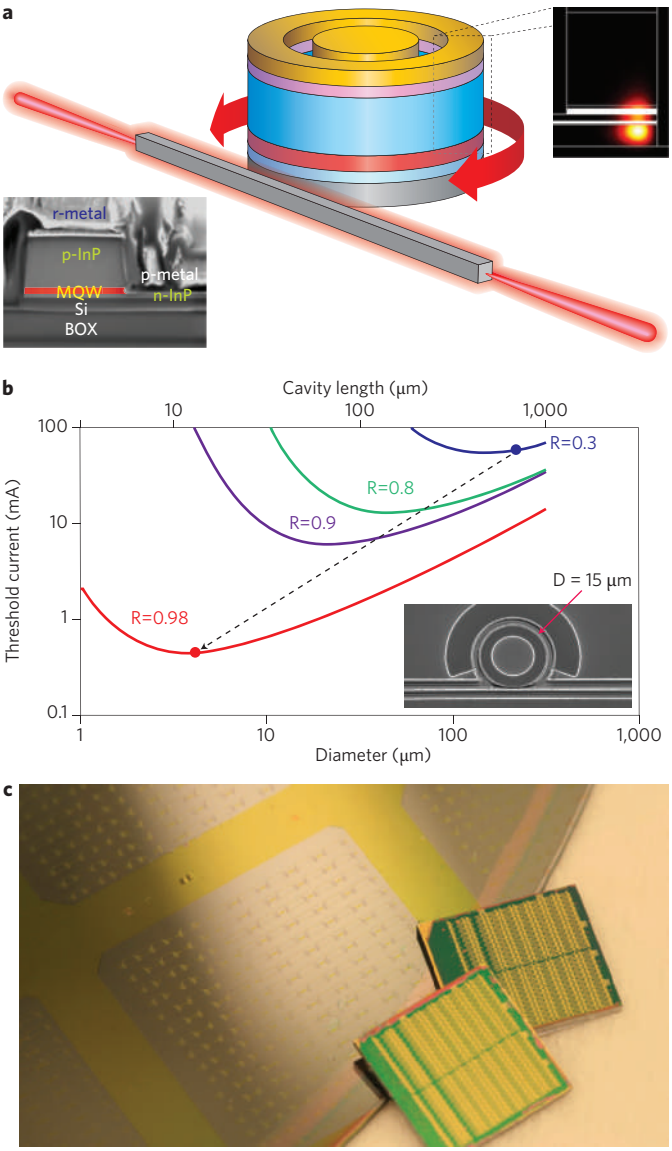

Figure 5 | Compact hybrid Si microring lasers. a, Schematic of a hybrid microring laser with a Si bus waveguide. Expanded view shows the simulated fundamental transverse electric mode shifting towards the waveguide edge. Inset: cross-sectional SEM image of a microring laser, showing the different layers and metal contacts. **b**, Calculated threshold current as a function of device cavity length for different facet reflectivities (*R*). Inset: top-view SEM image of a 15-μm-diameter device. **c**, A portion of a 150-mm-diameter III–V-on-SOI wafer containing ring cavity lasers (left) and 1 cm^2 chips containing 400 microring lasers (right).

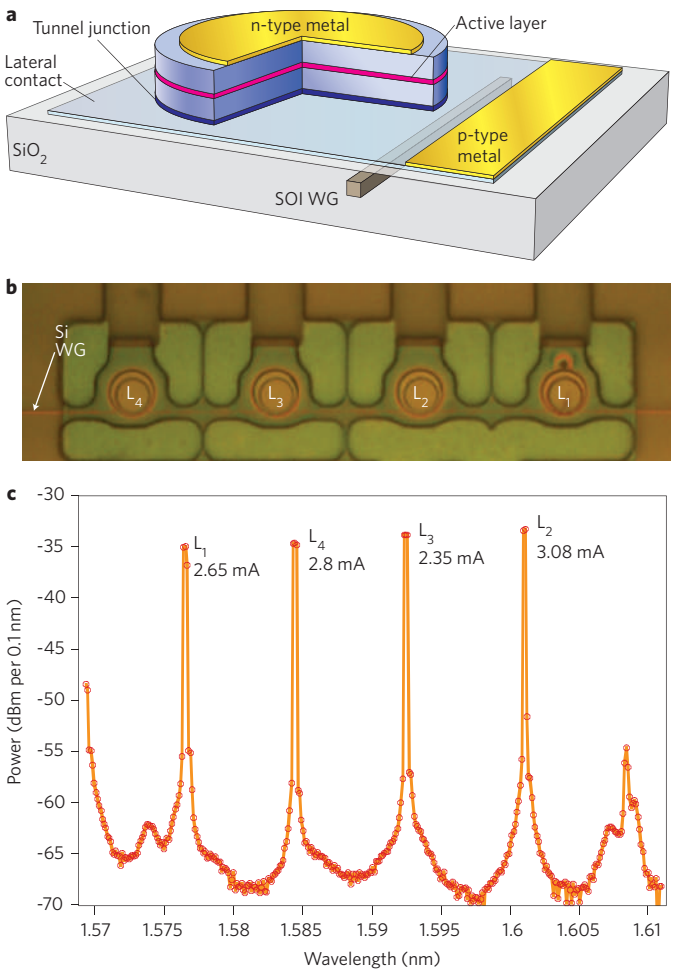

Figure 6 | Hybrid Si microdisk laser array. a, Schematic of a heterogeneously integrated III–V microdisk laser with a vertically coupled SOI waveguide (WG) underneath. **b**, Microscope image of the multiwavelength laser source consisting of four microdisk lasers (L_1–L_4) with slightly different disk diameters coupled to a common, underlying SOI waveguide. **c**, Balanced output spectrum obtained by adjusting the individual microdisk drive currents to get four evenly spaced wavelength channels. Figure reproduced with permission from ref. 60, © 2008 IEEE.

optical interconnect systems is likely to be a combination of hybrid and monolithic approaches, thus taking full advantage of III–V-, Ge- and Si-based materials. Integration with CMOS circuits can provide low cost, integrated control, signals processing and error correction. If Si photonics is to claim a large market in intrachip optical communication links, however, power consumptions must be reduced to 2 pJ bit^{-1} or lower[65].

Silicon Raman lasers are potentially ideal light sources for a variety of wavelength-sensitive regimes, owing to their unmatched wavelength purity and the possibility of extending the lasing wavelength into the mid-infrared region[66]. Example applications include high-resolution and ultrasensitive detection of molecules for trace gas analysis, pollution and toxic gas monitoring, biomedical sensing, coherent free-space optical communications and metrology[25]. Achieving mode-hop-free CW tuning without sacrificing linewidth and extinction ratio is relatively straightforward by tuning the emission wavelength of the pump laser. The sensing market is currently dominated by bulky and power-hungry solid-state and gas lasers, but Si Raman lasers will be very competitive in size and cost if a pump source can be integrated. Furthermore, recently demonstrated SiGe Raman amplifiers and lasers bring extra flexibility in the pump and signal wavelengths[67]. The higher carrier mobility in SiGe reduces the carrier lifetime and subsequently the FCA. Lasing realized in ring or disk resonators exhibits extremely useful resonance and nonlinear effects such as bistability. As shown in Fig. 5a, stimulated emission can propagate bidirectionally (that is, clockwise or anticlockwise). Multiple and single III–V ring lasers or hybrid disk lasers have been designed to realize flip-flop memory[68,69] and wavelength conversion[70]. When integrated on a single Si chip with low-loss Si or silica waveguides, Si ring/disk lasers promise to build ultrafast switches, buffers and complex nonlinear networks.

Silicon photonics is a rapidly evolving research field with tremendous potential. The term 'semiconductor lasers' now includes a broad range of approaches to lasers on silicon.

References

1. Soref, R. A. & Lorenzo, J. P. All-silicon active and passive guided-wave components for λ = 1.3 and 1.6 mm. *IEEE J. Quant. Electron.* **22,** 873–879 (1986).
2. http://www.itrs.net/
3. Pavesi, L. in *Device Applications of Silicon Nanocrystals and Nanostructures* (ed. Koshida, N.) Ch. 4 (Springer, 2009).
4. Bisi, O., Ossicini, S. & Pavesi, L. Porous silicon: a quantum sponge structure for silicon based optoelectronics. *Surf. Sci. Rep.* **38,** 1–126 (2000).
5. Gösele, U. & Lehmann, V. Light-emitting porous silicon. *Mater. Chem. Phys.* **40,** 253–259 (1995).
6. Canham, L. T. Silicon quantum wire array fabrication by electrochemical and chemical dissolution of wafers. *Appl. Phys. Lett.* **57,** 1046–1048 (1990).
7. Cullis, A. G. & Canham, L. T. Visible light emission due to quantum size effects in highly porous crystalline silicon. *Nature* **353,** 335–338 (1991).
8. Hirschman, K. D., Tsybeskov, L., Duttagupta, S. P. & Fauchet, P. M. Silicon-based visible light-emitting devices integrated into microelectronic circuits. *Nature* **384,** 338–341 (1996).
9. Wilson, W. L., Szajowski, P. F. & Brus, L. E. Quantum confinement in size-selected, surface-oxidized silicon nanocrystals. *Science* **262,** 1242–1244 (1993).
10. Pavesi, L., Dal Negro, L., Mazzoleni, C., Franzo, G. & Priolo, F. Optical gain in silicon nanocrystals. *Nature* **408,** 440–444 (2000).
11. Minoru, F., Masato, Y., Yoshihiko, K., Shinji, H. & Keiichi, Y. 1.54 mm photoluminescence of Er^{3+} doped into SiO_2 films containing Si nanocrystals: Evidence for energy transfer from Si nanocrystals to Er^{3+}. *Appl. Phys. Lett.* **71,** 1198–1200 (1997).
12. Iacona, F. *et al.* Silicon-based light-emitting devices: Properties and applications of crystalline, amorphous and Er-doped nanoclusters. *IEEE J. Sel. Top. Quant. Electron.* **12,** 1596–1606 (2006).
13. Lu, Z. H., Lockwood, D. J. & Baribeau, J. M. Quantum confinement and light emission in SiO_2/Si superlattices. *Nature* **378,** 258–260 (1995).
14. Cloutier, S. G., Kossyrev, P. A. & Xu, J. Optical gain and stimulated emission in periodic nanopatterned crystalline silicon. *Nature Mater.* **4,** 887–891 (2005).
15. Nassiopoulos, A. G., Grigoropoulos, S. & Papadimitriou, D. Electroluminescent device based on silicon nanopillars. *Appl. Phys. Lett.* **69,** 2267–2269 (1996).
16. Malinin, A., Ovchinnikov, V., Novikov, S., Tuovinen, C. & Hovinen, A. Fabrication of a silicon based electroluminescent device. *Materials Science and Engineering B* **74,** 32–35 (2000).
17. Pavesi, L. Routes toward silicon-based lasers. *Mater. Today* **8,** 18–25 (2005).
18. Pavesi, L. Silicon-based light sources for silicon integrated circuits. *Adv. Opt. Tech.* 416926 (2008).
19. Lee, K. K. *et al.* Effect of size and roughness on light transmission in a Si/SiO_2 waveguide: Experiments and model. *Appl. Phys. Lett.* **77,** 1617–1619 (2000).
20. Jalali, B. Making silicon lase. *Sci. Am.* 58–65 (February 2007).
21. Claps, R., Dimitropoulos, D., Han, Y. & Jalali, B. Observation of Raman emission in silicon waveguides at 1.54 μm. *Opt. Express* **10,** 1305–1313 (2002).
22. Boyraz, O. & Jalali, B. Demonstration of a silicon Raman laser. *Opt. Express* **12,** 5269–5273 (2004).
23. Jones, R. *et al.* Net continuous wave optical gain in a low loss silicon-on-insulator waveguide by stimulated Raman scattering. *Opt. Express* **13,** 519–525 (2005).
24. Rong, H. *et al.* A continuous-wave Raman silicon laser. *Nature* **433,** 725–728 (2005).
25. Rong, H. *et al.* Low-threshold continuous-wave Raman silicon laser. *Nature Photon.* **1,** 232–237 (2007).
26. Kawanami, H. Heteroepitaxial technologies of III–V on Si. *Sol. Energ. Mat. Sol. C.* **66,** 479–486 (2001).

27. Xie, Y. H., Wang, K. L. & Kao, Y. C. An investigation on surface conditions for Si molecular beam epitaxial (MBE) growth. *J. Vac. Sci. Tech. A* **3,** 1035–1039 (1985).
28. Samonji, K. *et al.* Reduction of threading dislocation density in InP-on-Si heteroepitaxy with strained short-period superlattices. *Appl. Phys. Lett.* **69,** 100–102 (1996).
29. Masafumi, Y., Mitsuru, S. & Yoshio, I. Misfit stress dependence of dislocation density reduction in GaAs films on Si substrates grown by strained-layer superlattices. *Appl. Phys. Lett.* **54,** 2568–2570 (1989).
30. Nozawa, K. & Horikoshi, Y. Low threading dislocation density GaAs on Si(100) with InGaAs/GaAs strained-layer superlattice grown by migration-enhanced epitaxy. *Jpn. J. Appl. Phys.* **30,** L668–L671 (1991).
31. Yamaichi, E., Ueda, T., Gao, Q., Yamagishi, C. & Akiyama, M. Method to obtain low-dislocation-density regions by patterning with SiO_2 on GaAs/Si followed by annealing. *Jpn. J. Appl. Phys.* **33,** L1442–L1444 (1994).
32. Groenert, M. E. *et al.* Monolithic integration of room-temperature cw GaAs/AlGaAs lasers on Si substrates via relaxed graded GeSi buffer layers. *J. Appl. Phys.* **93,** 362–367 (2003).
33. Groenert, M. E., Pitera, A. J., Ram, R. J. & Fitzgerald, E. A. Improved room-temperature continuous wave GaAs/AlGaAs and InGaAs/GaAs/AlGaAs lasers fabricated on Si substrates via relaxed graded Ge_xSi_{1-x} buffer layers. *J. Vac. Sci. Tech. B* **21,** 1064–1069 (2003).
34. Cerutti, L., Rodriguez, J. B. & Tournie, E. GaSb-based laser, monolithically grown on silicon substrate, emitting at 1.55 um at room temperature. *IEEE Photon. Tech. Lett.* **22,** 553–555 (2010).
35. Kunert, B., Volz, K., Koch, J. & Stolz, W. Direct-band-gap Ga(NAsP)-material system pseudomorphically grown on GaP substrate. *Appl. Phys. Lett.* **88,** 182108 (2006).
36. Kunert, B., Zinnkann, S., Volz, K. & Stolz, W. Monolithic integration of Ga(NAsP)/(BGa)P multi-quantum well structures on (001) silicon substrate by MOVPE. *J. Cryst. Growth* **310,** 4776–4779 (2008).
37. Yin, T. *et al.* 31 GHz Ge n-i-p waveguide photodetectors on silicon-on-insulator substrate. *Opt. Express* **15,** 13965–13971 (2007).
38. Kang, Y. *et al.* Monolithic germanium/silicon avalanche photodiodes with 340 GHz gain–bandwidth product. *Nature Photon.* **3,** 59–63 (2008).
39. Morse, M. *et al.* Monolithic Ge/Si avalanche photodiodes. *Proc. 6th IEEE Int. Conf. Group IV Photon.* 25–27 (2009).
40. Kuo, Y.-H. *et al.* Strong quantum-confined Stark effect in germanium quantum-well structures on silicon. *Nature* **437,** 1334–1336 (2005).
41. Roth, J. E. *et al.* Optical modulator on silicon employing germanium quantum wells. *Opt. Express* **15,** 5851–5859 (2007).
42. Liu, J. *et al.* Tensile-strained, n-type Ge as a gain medium for monolithic laser integration on Si. *Opt. Express* **15,** 11272–11277 (2007).
43. Sun, X., Liu, J., Kimerling, L. C. & Michel, J. Room-temperature direct bandgap electroluminescence from Ge-on-Si light-emitting diodes. *Opt. Lett.* **34,** 1198–1200 (2009).
44. Cheng, S.-L. *et al.* Room temperature 1.6 μm electroluminescence from Ge light emitting diode on Si substrate. *Opt. Express* **17,** 10019–10024 (2009).
45. Liu, J., Sun, X., Camacho-Aguilera, R., Kimerling, L. C. & Michel, J. Ge-on-Si laser operating at room temperature. *Opt. Lett.* **35,** 679–681 (2010).
46. Jambois, O. *et al.* Current transport and electroluminescence mechanisms in thin SiO_2 films containing Si nanocluster-sensitized erbium ions. *J. Appl. Phys.* **106,** 063526 (2009).
47. Jambois, O. *et al.* Towards population inversion of electrically pumped Er ions sensitized by Si nanoclusters. *Opt. Express* **18,** 2230–2235 (2010).
48. Liang, D. & Bowers, J. E. Highly efficient vertical outgassing channels for low-temperature InP-to-silicon direct wafer bonding on the silicon-on-insulator (SOI) substrate. *J. Vac. Sci. Tech. B* **26,** 1560–1568 (2008).
49. Pasquariello, D. & Hjort, K. Plasma-assisted InP-to-Si low temperature wafer bonding. *IEEE J. Sel. Top. Quant. Electron.* **8,** 118–131 (2002).
50. Park, H., Fang, A. W., Kodama, S. & Bowers, J. E. Hybrid silicon evanescent laser fabricated with a silicon waveguide and III–V offset quantum wells. *Opt. Express* **13,** 9460–9464 (2005).
51. Roelkens, G., Van Thourhout, D., Baets, R., Notzel, R. & Smit, M. Laser emission and photodetection in an InP/InGaAsP layer integrated on and coupled to a silicon-on-insulator waveguide circuit. *Opt. Express* **14,** 8154–8159 (2006).
52. Fang, A. W. *et al.* Electrically pumped hybrid AlGaInAs-silicon evanescent laser. *Opt. Express* **14,** 9203–9210 (2006).
53. Fang, A. W. *et al.* Integrated AlGaInAs-silicon evanescent race track laser and photodetector. *Opt. Express* **15,** 2315–2322 (2007).
54. Fang, A. W. *et al.* A distributed Bragg reflector silicon evanescent laser. *IEEE Photon. Tech. Lett.* **20,** 1667–1669 (2008).
55. Fang, A. W., Lively, E., Kuo, Y.-H., Liang, D. & Bowers, J. E. A distributed feedback silicon evanescent laser. *Opt. Express* **16,** 4413–4419 (2008).
56. Van Campenhout, J. *et al.* Electrically pumped InP-based microdisk lasers integrated with a nanophotonic silicon-on-insulator waveguide circuit. *Opt. Express* **15,** 6744–6749 (2007).
57. Liang, D. *et al.* Hybrid silicon (λ=1.5 mm) microring lasers and integrated photodetectors. *Opt. Express* **17,** 20355–20364 (2009).
58. Liang, D. *et al.* High-quality 150 mm InP-to-silicon epitaxial transfer for silicon photonic integrated circuits. *Electrochem. Solid. Lett.* **12,** H101–H104 (2009).
59. Spuesens, T. *et al.* Improved design of an InP-based microdisk laser heterogeneously integrated with SOI. *Proc. 6th IEEE Int. Conf. Group IV Photon.* 202–204 (2009).
60. Van Campenhout, J. *et al.* A compact SOI-integrated multiwavelength laser source based on cascaded InP microdisks. *IEEE Photon. Tech. Lett.* **20,** 1345–1347 (2008).
61. Sysak, M. N. *et al.* Experimental and theoretical thermal analysis of a hybrid silicon evanescent laser. *Opt. Express* **15,** 15041–15046 (2007).
62. Fedeli, J. M. *et al.* Development of silicon photonics devices using microelectronic tools for the integration on top of a CMOS wafer. *Adv. Opt. Tech.* 412518 (2008).
63. Chang, H.-H. *et al.* Integrated triplexer on hybrid silicon platform. *Optical Fiber Communication Conf.* paper OThC4 (2010).
64. Sysak, M. N., Anthes, J. O., Bowers, J. E., Raday, O. & Jones, R. Integration of hybrid silicon lasers and electroabsorption modulators. *Opt. Express* **16,** 12478–12486 (2008).
65. Miller, D. A. B. Device requirements for optical interconnects to silicon chips. *Proc. IEEE* **97,** 1166–1185 (2009).
66. Soref, R. Toward silicon-based longwave integrated optoelectronics (LIO). *Proc. SPIE* **6898,** 689809 (2008).
67. Claps, R. *et al.* Raman amplification and lasing in SiGe waveguides. *Opt. Express* **13,** 2459–2466 (2005).
68. Hill, M. T. *et al.* A fast low-power optical memory based on coupled micro-ring lasers. *Nature* **432,** 206–209 (2004).
69. Liu, L. *et al.* An ultra-small, low-power, all-optical flip-flop memory on a silicon chip. *Nature Photon.* **4,** 182–187 (2010).
70. Raz, O. *et al.* Compact, low power and low threshold electrically pumped micro disc lasers for 20Gb/s non return to zero all optical wavelength conversion. *Optical Fiber Communication Conf.* paper OMQ5 (2010).

Acknowledgements

The authors thank Scott Rodgers, Ron Esman, Mike Haney and Jag Shah of DARPA/MTO, the Kavli Foundation, Intel and Hewlett Packard for funding this research. Many others contributed to the hybrid silicon research described here, including Hanan Bar, Dan Blumenthal, Hsu-Hao Chang, Hui-Wen Chen, Alexander Fang, Hyundai Park, Martijn Heck, Richard Jones, Brian Koch, Mario Paniccia, Omri Raday and Matthew Sysak.

Additional information

The authors declare competing financial interests: details accompany the paper at www.nature.com/naturephotonics.